RSC Advances

PAPER

View Article Online
View Journal | View Issue

Cite this: *RSC Adv.*, 2026, **16**, 5336

Application of poly-DL-methionine/gold nanoparticle-modified recycled battery graphite as an eco-friendly electrochemical sensor for the spasmolytic drug vincamine

Naglaa Abdel Sattar Kabil,[a] Nada Mousad Refay,[a] Yasmine Ahmed Sharaf,[a] Hisham Ezzat Abdellatef[a] and Rasha M. El Nashar *[b]

Received 23rd September 2025
Accepted 23rd December 2025

DOI: 10.1039/d5ra07233f

rsc.li/rsc-advances

The present work suggests the use of an economic, ultra-sensitive, and sustainable electrochemical sensor based on the electropolymerization of DL-methionine as a conducting polymeric film on a gold nanoparticle-modified battery graphite electrode, poly(DL-met)/AuNPs-BGE, for the analysis of vincamine (VIN), a natural alkaloid spasmolytic drug used for managing Alzheimer's, neurodegenerative, and normal aging-related cognitive diseases. The sensor exhibited a broad linear working range from 0.003 to 100 μM (R^2 = 0.9985), with a low detection limit of 0.00046 μM, and considerable repeatability and reproducibility results. The presented approach was applied effectively for VIN quantification in the pharmaceutical dosage formulation, spiked human urine, and plasma samples with good recovery ranges of 95.78–101.20% and low RSD values of 1.51–1.62% (n = 3), showing the suggested sensor's reliability and efficiency for selective analysis of VIN in various matrices. Additionally, the sustainability of the method was verified utilizing different analytical greenness metrics, in addition to the very recent blue applicability grade index (BAGI).

1. Introduction

Vincamine (VIN), with the chemical name eburnamenine-14-carboxylic acid, 14,15-dihydro-14-hydroxy-, methyl ester (3α,14β,16α), is a natural alkaloid obtained from *Vinca minor* leaves, which has been recently introduced in the BP in 2021. It has been widely used for decades as a nootropic or memory enhancer for managing neurodegenerative diseases, Alzheimer's disease, or normal aging-related cognitive decline due to cerebrovascular insufficiency. It acts as a selective vasoregulatory agent for the microcapillary circulation. VIN significantly enhances the cerebral metabolism by increasing the regional circulation, ATP generation, and the uptake of glucose and oxygen by ischemic cerebral zones.[1] VIN also has vital antioxidant and anti-inflammatory activities, making it a promising and efficient therapeutic agent for various inflammatory conditions throughout the body.[2,3] Additionally, it shows promise in managing chronic hyperglycaemia by improving glucose control and lipid profiles.[4]

In the realm of cancer treatment, VIN has lately been investigated for its cancer-fighting abilities, showing an effective, affordable, and safe anti-tumor activity.[5] Ventricular tachycardia was reported as an adverse effect of vincamine's extensive use, which often results in sudden loss of awareness and may lead to sudden death.[6] Accordingly, the analysis of VIN as a precious herbal medicine in pharmaceuticals and biological fluids plays a crucial role in establishing drug specifications, monitoring chemical quality criteria, investigating toxicity of long-term administration, and its regular control.

Based on the literature, several methods were employed for VIN quantification, including chromatographic,[7–9] LC/MS,[10] spectrophotometric,[7,11,12] spectrofluorimetric[11,13] and capillary electrophoretic[14] techniques. Despite their wide applicability in the industrial and quality control of pharmaceutical compounds, chromatographic methods require qualified operators, hazardous solvents that have a negative impact on the ecosystem, and high-cost instrumentation, while spectroscopic methods are time-consuming and have limited sensitivity and selectivity; thus, both techniques require tedious and complicated sample pre-treatment procedures and, therefore, are not appropriate for *in situ* analysis.

Compared to the other analytical detection techniques, electrochemical methods of analysis offer significant advantages in terms of reliability, simplicity, accessibility, facile operation, rapid response, minimal waste, low cost, miniaturization, and instantaneous, ultra-sensitive, and selective analysis of the target analyte in diverse samples without any preliminary preparation.[15]

[a]*Analytical Chemistry Department, Faculty of Pharmacy, Zagazig University, Zagazig 44519, Egypt*

[b]*Chemistry Department, Faculty of Science, Cairo University, Giza, 112631, Egypt. E-mail: rasha.elnashar@cu.edu.eg; rashaelnashar@gmail.com*

Only a few electrochemical techniques have been published for VIN detection. The earlier detection method involves the use of a Nujol-based carbon paste electrode and adsorptive stripping voltammetric technique (SW-AdSV), which requires potential controlled pre-concentration and stripping procedures.[16] While in another study, VIN was detected in 0.1 M B–R buffer, on a bare glassy carbon electrode (GCE) by means of differential pulse and square wave voltammetry (DPV and SWV). It is clear that the developed voltammetric methods were carried out on unmodified electrodes with the drawbacks of a high background current, slow redox kinetics, and poor selectivity.[17] To address this issue, it was critical to develop a chemically modified electrode for performance and analytical capabilities improvement of VIN voltammetric detection. No reported method for VIN involves the use of disposable graphite rods as a working electrode (GE), although they can be obtained from recyclable sources such as waste batteries instead of costly commercial electrodes as the GCE.

Currently, the demand for batteries is urgent for matching with massive technology; therefore, huge quantities of battery waste are generated. Zinc–carbon batteries remain one of the most prevalent types, largely due to their low cost, abundant raw materials, and simple fabrication technology. Waste zinc–carbon (Zn–C) batteries constitute a valuable secondary resource owing to their recoverable metallic components and aqueous concentrated electrolyte solutions of zinc and ammonium chlorides. Additionally, this battery type has been exploited as a precursor for carbon nanoparticle materials and graphene synthesis, a material with broad technological relevance especially for supercapacitors.[18,19] Spent electrodes from these batteries can also be upcycled into high-performance $LiMn_2O_4$ cathodes and carbon (graphite) anodes for use in lithium-ion battery systems.[20]

The recycling of spent batteries can also contribute to minimizing electronic waste, as wrongfully disposed batteries are considered special residues due to the leaching of large quantities of zinc, manganese, and other heavy metals into the ecosystem, which have devastating impacts on living species, the environment, and human health owing to their bioaccumulative and largely emissive nature.[21]

One effective approach for reusing waste batteries involves utilizing recovered graphite as a sensor.[22,23] Graphite material is chemically inert, possesses excellent electrical conductivity, and has a unique structure that can be modified easily.[24,25] For example, graphite powder recovered from spent batteries and carbon nanotubes, modified with tartrazine, has been evaluated for dopamine detection.[26] Furthermore, electrochemically reduced graphene oxide films deposited on GCE, synthesized using graphite obtained from discharged Zn–C batteries, have demonstrated effective performance in determining hydroquinone and paracetamol.[27] Additionally, the battery graphite electrodes (BGE), employing the recovered graphite rods possess perfect size, lightweight, large surface area, good mechanical stiffness, and sustainability; furthermore, they require only a few non-tedious pre-treatment procedures at a much lower temperature than the carbon paste electrode (CPE), are modifiable, and display clearly defined and reproducible voltammetric signals over a wide potential range, making them promising electrochemical sensors.[24,28–30]

Chemically modified electrodes exhibit improved sensitivity, stability, selectivity, and catalytic response compared to bare electrodes. Various conducting materials such as metal nanoparticles (MNPs),[31] carbon nanotubes (CNTs),[32] metal oxides,[33,34] metal sulphides,[35] conducting polymers,[36] and DNA-doped polymers[37] have been utilized for this purpose.

Gold nanoparticles (AuNPs) are one of the most applied and pioneering nanomaterials due to their unique physicochemical attributes, excellent electrocatalytic ability, high conductivity, stability, and biocompatibility, making them precious scaffolds for superior overall performance in electroanalytical, catalytic, and biomedical domains.[38–40] In comparison to chemical synthesis, electrochemical deposition offers a more environmentally friendly, time- and labor-saving alternative for yielding AuNPs with a smaller particle size, more ordered distribution, and higher purity.[41] Therefore, AuNP-surface modification of sensors by means of electrodeposition, such as cyclic voltammetry, linear sweep voltammetry, or chronoamperometry at a fixed potential, as previously reported,[42] results in the formation of a stable and dense sensing film, which enhances the electron transfer kinetics and minimizes the impedance at the interface between the electrode and the electrolyte.

Recently, conducting polymers (CPs) have been widely employed in various fields, with an emphasis on biosensors,[43] artificial muscles,[44] biofuel cells,[43] supercapacitors,[45] and microelectronics.[46] CPs are a class of electrically conductive, functional polymers that are fundamentally organic. They have superior properties to typical organic polymers in terms of selectivity, electron affinity, redox activity, and electroconductivity, which enable them to serve as potential interfacial modification materials in electrochemical sensing.[47] Electropolymerization is an intriguing option for immobilizing the conductive polymers on the sensor surface due to facile operation, precise control over membrane thickness and surface coverage, an easily adjustable potential window, as well as possible application to a wide range of electrode materials.[48]

Combining AuNPs and conducting polymers in the fabricated sensing layer of electrochemical sensors has gained enormous attention in recent years due to the ease of interaction and facile dispersion of AuNPs within the CP porous structure, offering homogenous polymeric films with more electroactive sites and a stabilized nanomaterial film.[36,49] The numerous noteworthy benefits of amino acid-based polymers (biomolecules) such as high catalytic activity, self-assembly in ordered patterns, electrochemical stability, environmental friendliness, and facilitated electropolymerization due to the presence of $–NH_2$ and –COOH groups into their structure potentiated their intensive use for diverse sensors' surface modification.[50]

One of the amino acids employed for sensor's surface pretreatment is DL-methionine (DL-met), a sulfur-containing amino acid that can be prepared in a phosphate buffer solution, pH 7.0, and electropolymerized applying cyclic voltammetry (CV) at a potential ranging from −0.6 to 2.0 V, forming a porous conducting polymeric layer with a considerable number of active sites.[37] The –S moieties and $–NH_2$ groups in poly(DL-met) can

coordinate AuNPs on the electrode surface, forming a macrochelate structure through chemical binding (Au–S and Au–N bonds).[51,52]

The present work aims to establish a selective, sustainable, and cost-effective voltammetric technique for the detection of VIN in pharmaceutical formulations, spiked human plasma, and urine samples utilizing an affordable graphite sensor and biocompatible reagents. The interfacial sensing layer of the employed recyclable BGE was decorated with poly(DL-met)/AuNPs to take advantage of their synergistic catalytic characteristics, which, in turn, improve both the sensitivity and selectivity of the sensor. The proposed approach was validated for accuracy, precision, stability, and selectivity, as stated by the ICH. Greenness and blueness metrics were employed for evaluating the sustainability profile of the suggested method in highlight of the applied operational and design parameters.

2. Experimental

2.1. Instrumentation and software

Using PSTrace5 software version 5.8.1704, the Palmsens4 EIS Potentiostat/Galvanostat (PalmSens BV, Houten, Netherlands) was employed to perform all of the electrochemical measurements. The working, reference, and counter electrodes in this three-electrode system were a 3 mm-diameter battery graphite rod from a recycled AAA carbon zinc battery, Ag/AgCl, and a 1 mm-diameter platinum wire. pH adjustments were carried out utilizing a Jenway digital pH meter, model 3510 (Jenway Instruments, Staffordshire, UK). A field emission-scanning electron microscope (FESEM, FEI, USA) equipped with an energy-dispersive X-ray spectroscopy (EDX) detector was employed to investigate the surface morphology and the elemental composition of the modified electrode surface. An Agilent atomic force microscopic (AFM) system 5600 Ls (Agilent Technologies, Inc., Santa Clara, CA, USA) was used to characterize the surface's topography.

2.2. Materials and reagents

Without undergoing additional purification, all of the reagents utilized in this work were of analytical grade. A VIN standard with a certified purity of 99.78% was kindly obtained from Amoun Pharmaceutical Co. (Obour City, Egypt). BRAIN-OX® capsules, 30 mg VIN/capsule, were manufactured by October Pharma (6th of October City, Egypt). Gold(III) chloride trihydrate 99.9%, DL-methionine (DL-met) ≥99%, sulfuric acid 98%, hydrochloric acid 36%, phosphoric acid 85%, glacial acetic acid, boric acid, sodium hydroxide, anhydrous potassium dihydrogen phosphate, dipotassium hydrogen orthophosphate, potassium ferrocyanide trihydrate, potassium ferricyanide, and potassium chloride were acquired from Sigma-Aldrich (Hamburg, Germany). The pure lab UHQ system (ELGA, High Wycombe, UK) was utilized to purify water (Milli-Q) used throughout the investigation.

2.3. Preparation of solutions

A stock solution of VIN (1.0 mM) was prepared in 0.1 M HCl and 0.1 M Britton–Robinson (B–R) buffer (pH = 6.0) with a ratio of 1 : 3 and then diluted in the B–R buffer to the required concentrations of working standards for the quantitative analysis, 3.0×10^{-9} to 1.0×10^{-4} M (1.08 ng mL^{-1}–35.44 μg mL^{-1}) VIN solutions. After that, 0.1 M B–R buffer of pH 2.0–12.0 was prepared by dissolving boric acid (6.184 g) in ultra-pure water, and acetic acid (5.77 mL) and phosphoric acid (6.81 mL) were added; NaOH solution (0.2 M) was utilized for the pH adjustment, and then, the final volume was adjusted with Milli-Q water (1.0 L). A DL-met (2.5 mM) solution was prepared by dissolving 0.01 g DL-met in 25 mL phosphate buffer solution (0.1 M PBS, pH 7.0), which was prepared by using 5.323 g of potassium dihydrogen phosphate anhydrous and 1.896 g of dipotassium hydrogen orthophosphate, dissolved in Milli-Q water (500 mL). Then, a 5 mM $[Fe(CN)_6]^{3-}$/$[Fe(CN)_6]^{4-}$ solution was prepared by adding 0.211 g of potassium ferrocyanide trihydrate and 0.1645 g of potassium ferricyanide to 100 mL solution of 0.1 M KCl (0.745 g) prepared in ultrapure water. All stock solutions were stored in dark bottles at 4 °C until use.

2.4. Fabrication of the working electrode

From the depleted AAA zinc–carbon batteries, the graphite rods were cautiously removed. After recovery, the rods were cleaned with paper towels and consequently ultrasonically cleansed with 0.5 M H_2SO_4 and Milli-Q water for 20 min to remove any adhesive particulates of the zinc paste.[53] After that, the graphite rods were dried in an oven for 24 hours at 120 °C to completely remove moisture. The tip was mechanically polished with P130-grit emery paper, then with P1000 and P2000 grades, followed by polishing with 1.0, 0.30, and 0.05 μm alumina slurry till obtaining a mirror-like surface. The rods were then sealed with a dielectric shrink PTFE tape and heat-treated in an oven at 60 °C to ensure that the tape shrinks and fits the electrode body to insulate the graphite rod from the side.

Until use, the fabricated battery graphite electrode (BGE) was stored at ambient temperature, and as a preparatory cleaning and activation step to improve their electrochemical characteristics, BGEs were exposed to cyclic voltammetric (CV) scanning in 0.1 N NaOH at a scan rate of 0.1 V s^{-1} and a potential ranging from −0.5 V to 1.5 V until a stable signal was achieved, rinsed with ultrapure water and then dried before each measurement.[54]

2.5. Experimental parameter optimization

Different operational variables, including Au-deposition time, concentration of DL-met, number of electropolymerization cycles, pH of the electrolyte solution, accumulation time, accumulation potential, and potential step, were investigated to recognize the ideal operating levels influencing the response of the fabricated sensor towards 10 μM VIN applying the DPV technique.

2.6. Electrode' modification

In accordance with earlier reports on AuNP deposition, chronoamperometry (*i*–*t*) was the applied technique[21,36] after submerging BGE in a 0.5 M H_2SO_4 solution containing 0.01 g mL^{-1} of $HAuCl_4 \cdot 3H_2O$ at a fixed potential of −0.4 V for

various deposition time intervals from 30 to 180 s with increments of 30 s. The electrode was then rinsed with distilled water and set aside to dry at the ambient temperature. Following that, various concentrations covering the range of 0.5–5.0 mM of DL-met in 0.1 M PBS, pH 7.0, and varying numbers of electropolymerization cycles (3–12 cycles) were studied for the formation of an optimized coating film of poly(DL-met) on the modified sensor surface (AuNPs-BGE) using cyclic voltammetry at a potential ranging from −0.6 V to 1.5 V and a scan rate of 0.1 V s^{-1}.[55] Finally, any unreacted methionine was removed from the sensor surface by soaking in distilled water, which was then kept dry until use.

2.7. Interference study

The impact of possible interference was examined by comparing the current response of poly(DL-met)/AuNPs-BGE towards pure VIN with that for a mixture of VIN and possible interfering constituents such as other memory enhancers that may be co-formulated or prescribed with VIN as piracetam, donepezil, and memantine; its structurally related synthetic derivative is vinpocetine and other co-administered drugs include pantoprazole and vitamin B12. Three VIN-containing mixtures were made for each examined interferent, with the interferent concentration equal to ten times or 100 times that of VIN.

2.8. Analytical application

VIN was measured in a variety of matrices, such as pharmaceutical formulations, spiked urine, and plasma samples, to validate the reliability and applicability of the developed procedures.

For pharmaceutical formulation sampling, ten BRAIN-OX® capsules were emptied, their contents were weighed and finely powdered, the amount equivalent to one capsule (30 mg VIN) was transferred into a 50 mL volumetric flask containing 15 mL of 0.1 M HCl, the obtained mixture was subjected to sonication for 15 min and subsequently filtered through 0.45 μm (ultrapure) PTFE. The volume was made up to the mark with B–R buffer of pH 6.0 to obtain a stock solution (600 μg per mL VIN). The stock solution was serially diluted in 0.1 M B–R of pH 6.0 to prepare the required concentrations, and DP voltammograms were recorded under the optimized conditions.

As renal excretion is the main route for VIN elimination,[56] the developed sensor capability to accurately and selectively measure VIN in human urine samples was estimated. Urine samples (10 mL) were collected from healthy anonymous individuals and passed through PTFE (0.45 μm) before mixing with 0.1 M B–R buffer (pH 6.0) (1 : 50) without any additional pretreatment steps. The diluted urine samples were spiked with various concentrations of VIN to the final concentrations of 1.78, 3.54, and 17.76 ng per mL VIN solutions.

Aliquots of human plasma (100 μL) were spiked with different concentrations of VIN and vortexed for 2 minutes. Protein precipitation was achieved by adding 1 mL of methanol, followed by another step of vortexing for 2 minutes. The samples were then centrifuged at 10 000 rpm for 5 minutes. The resulting supernatants were filtered, and the filtrates were transferred to 10 mL volumetric flasks and diluted to required volumes with a buffer to obtain the final required concentrations of 1.78, 3.54, and 17.76 ng mL^{-1}.

3. Results and discussion

3.1. Optimal fabrication conditions for the sensor

The sensor performance can be enhanced through optimizing the various experimental parameters that impact its response towards VIN, such as AuNP deposition time, monomer concentration, the number of electropolymerization cycles, and the pH of the electrolyte supporting medium, as well as the DPV variables such as step potential, accumulation time, and accumulation potential, as the most influential electrochemical parameters.

3.1.1. Impact of the AuNPs' electrodeposition time. The sensor surface was decorated with AuNPs at various deposition time intervals ranging from 30 to 180 s with increments of 30 s prior to DL-met electropolymerization, applying chronoamperometric technique in an aqueous solution of 0.03 M $HAuCl_4$ precursor prepared in 0.5 M H_2SO_4, and the peak current responses (I_P) for 10 μM VIN on the surface of AuNPs-BGEs were monitored and compared with the I_P response on using the bare BGE.

The oxidation peak current was noticed to be gradually increased with time, reflecting the successful deposition of AuNPs on the electrode surface, and the maximum I_P was achieved at 120 s, after which a gradual decrease in current was observed, as demonstrated in Fig. 1(A), which may be due to the excessive clustering of AuNPs on the sensor surface that act as a block hindering the flow of electrons.[57] When compared to the bare BGE, AuNPs were noticed to boost the sensitivity of the BGE, as evident from the elevation of the I_P by almost twenty times; this can be explained by the larger surface area and improved kinetics of electron transfer.[55]

3.1.2. Optimizing the concentration of monomers (DL-met). Since the concentration of monomers in the polymerization mixture might impact the formed polymeric film thickness and, consequently, the surface conductivity, the effect of the monomer's concentration on the oxidation peak of VIN was investigated. Various monomer concentrations, covering the range of 0.5–5.0 mM in PBS of pH 7.0, were tested while other variables were held constant, including Au deposition time (120 s), the number of polymerization cycles (3 cycles), the potential scan rate of 0.1 V s^{-1} over the range of −0.6 to 1.5 V, and the pH (6.0) of the electrolyte solution, and the consequent I_P responses for 10 μM VIN were then recorded.

The electrode response (I_P) was observed to increase while increasing the monomer concentration, which then peaked at 2.5 mM of DL-met, as indicated in Fig. 1(B). Following this, the I_P gradually declined, which could be attributed to the formation of a thicker and less porous polymeric membrane with reduced conductivity.[37,58]

3.1.3. DL-Met electropolymerization. The polymeric film's thickness can be regulated by changing the number of polymerization scans. A dense insulating layer may form on the surface of a sensor after a large number of cycles, hindering the

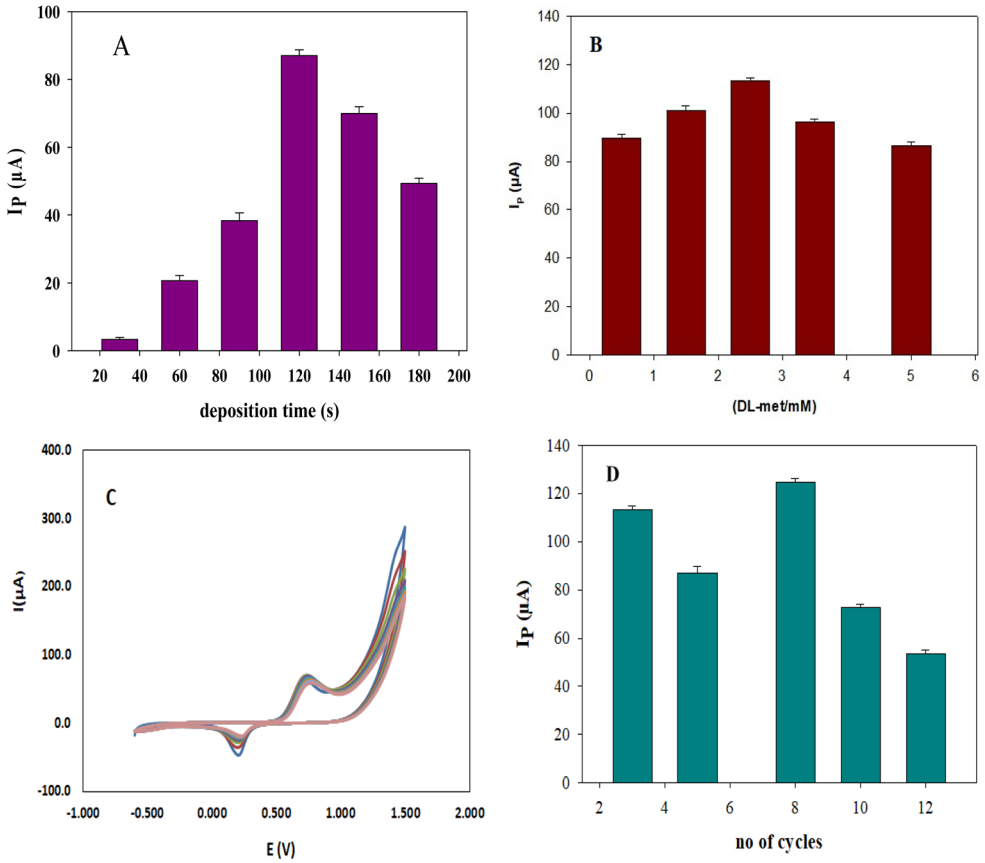

Fig. 1 (A) Effect of AuNP deposition time. (B) Effect of the DL-methionine concentration. (C) CV scans from −0.6 to 1.5 V at 0.1 V s^{-1} scan rate for 8 cycles for the electropolymerization of DL-methionine (2.5 mM) prepared in PBS (0.1 M) pH 7. (D) Effect of the number of electropolymerization cycles of DL-methionine on the response of the fabricated BGE towards a 10 μM VIN solution prepared in a 0.1 M B–R buffer, pH 6.

diffusion process. Moreover, a low cycle count may result in thin and fragile film formation;[15] therefore, it is critical to maximize the sensor performance *via* proper selection of the optimal number of deposition cycles.

Cyclic voltammetry (CV) was applied for DL-met (2.5 mM in 0.1 M PBS, pH 7.0) electropolymerization on a AuNP-modified BGE at a potential in the range of −0.6 V to 1.5 V using a scanning speed of 0.1 V s^{-1} for varying numbers of polymerization cycles (3–12 cycles). As represented in Fig. 1(C), an oxidation signal was noticed at ~0.8 V in the initial electropolymerization scan, which was displaced to less positive potential over the subsequent scans, signifying the development of a coating film of poly(DL-met) on the AuNPs-BGE surface. Eight polymerization cycles were recorded to be optimal, producing the maximum I_P for VIN, and further increases resulted in a drop in the current signal. This may be ascribed to the declined sensitivity and conductivity of the Au-modified BGE due to the formation of a dense polymeric layer, as displayed in Fig. 1(D).

3.2. Optimization of the experimental variables

3.2.1. Working pH range. The most appropriate pH value was investigated for realizing the maximum accuracy and reliability of measurements, using poly(DL-met)/AuNPs-BGE immersed in 10 μM VIN prepared in a 0.1 M B–R buffer over a working pH range from 3.0 to 10.0, at a scan rate of 50 mV s^{-1}. Throughout the examined pH range, a single, clearly defined anodic peak was observed, with the peak current intensity being maximized at pH 6.0.

Fig. 2(A) represents the I_P responses for 10 μM VIN within the examined pH range. Obtaining high peak currents at pH values (6.0–7.0) can be explained by the protonation state of vincamine, which promotes optimal proton-coupled electron transfer (pK_a = 6.172), which results in a facilitated oxidation kinetics. The current response was sharply declined at the highly acidic and alkaline pH values, which could be attributed to the instability of VIN in a highly acidic or alkaline medium.[59]

Moreover, it was found that the peak potential (E_p) for VIN oxidation is significantly influenced by the working pH value. As the pH has increased, the peak potential has moved to less positive levels, verifying the pH dependence and direct participation of protons in the proposed redox process.[17]

To have a more profound understanding of the redox reaction of VIN, the correlation between pH and oxidation peak potential was graphed (Fig. 2(B)) to identify the electron-transfer mechanism. The derived equation demonstrated that the anodic peak potential for VIN oxidation exhibits a linear pH dependence using the suggested poly(DL-met)/AuNPs-BGE. The regression line equation eqn (1) was found to be

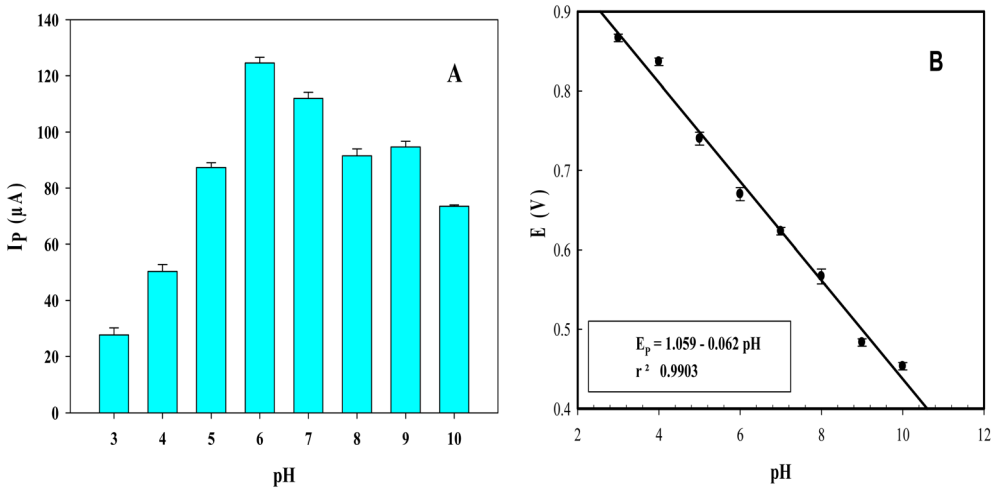

Fig. 2 (A) Effect of pH on the anodic peak current of 10 μM VIN solution prepared in a 0.1 M B–R buffer solution. (B) The regression analysis of pH and the anodic peak potential relationship using a 10 μM VIN solution prepared in a 0.1 M B–R buffer solution.

$$E_p = 1.059 - 0.062\ \text{pH} \quad R^2 = 0.9903,\ (\text{pH } 3.0\text{–}10.0) \qquad (1)$$

Philip Rieger's equation (eqn (2)), which clarifies the relation between the number of protons and electrons participating in the redox reaction, was matched with eqn (1):[60,61]

$$E_p = k - (0.059\ y/n)\ \text{pH} \qquad (2)$$

where k, y, and n represent the intercept of the regression line, number of protons, and number of electrons employed in the electrochemical process, respectively. It was noticed that the derived slope value of 0.062 (eqn (1)) is quite similar to the ideal slope of 0.059 (eqn (2)), indicating that the y/n ratio approaches unity, suggesting that the irreversible oxidation reaction of VIN involves an equal number of protons and electrons, as reported previously.

Based on the structure of VIN, the electro-oxidation mechanism for VIN could be attributed to the oxidation of the tertiary amine moiety *via* a one-electron transfer, accompanied by the liberation of one proton as expressed by eqn (3). These observations coincide with earlier studies concerning the oxidation of tertiary amine derivatives.[62]

3.2.2. DPV operational parameters. Several operational variables, including step potential (E_s), accumulation time (t_{acc}), and accumulation potential (E_{acc}), which are considered to be the most crucial DPV parameters, were examined to achieve the best operational performance of poly(DL-met)/AuNPs-BGE for the detection of 10 μM VIN applying a pulse width of 0.02 s, a pulse amplitude of 0.2 V, a scan rate of 0.05 V s^{-1}, and constant previously optimized measurement variables. The E_s value shifted between 0.005 V and 0.03 V; the magnitude of the oxidation current peaked at a potential step of 0.025 V, as shown in Fig. 3(A).

The accumulation time (t_{acc}) and potential (E_{acc}) may have a noticeable impact on the sensor performance, as they influence the deposited analyte amount onto the electrode surface and, in turn, the limit of detection.[63] T_{acc} was studied from 2 to 120 s just before the measurements; after 3 minutes of incubation of the fabricated electrode in 10 mM VIN and B–R buffer of pH 6.0, the highest current intensity was attained by applying a negligible t_{acc} of 2 s, as shown in Fig. 3(B). This can be attributed to the saturation of the sensor surface with the maximum amount of VIN molecules as a result of the accelerated rate of electron transfer, indicating the effective sensor modification. Accordingly, no accumulation time was applied.

Additionally, E_{acc} was varied from 0 to 0.04 V. As presented in Fig. 3(C), the maximum I_P value was noticed at zero (E_{acc}), the increase in E_{acc} starting from 0.01 V resulted in a drop in I_P. Therefore, no E_{acc} was applied.

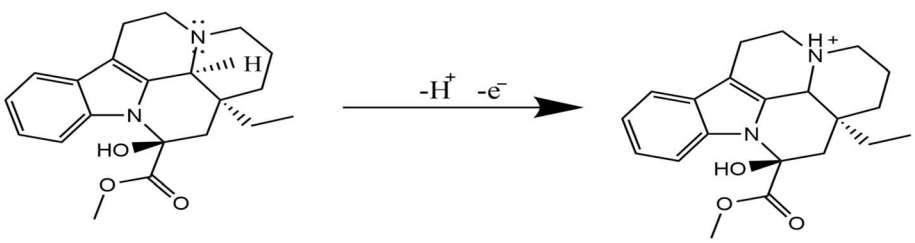

(3)

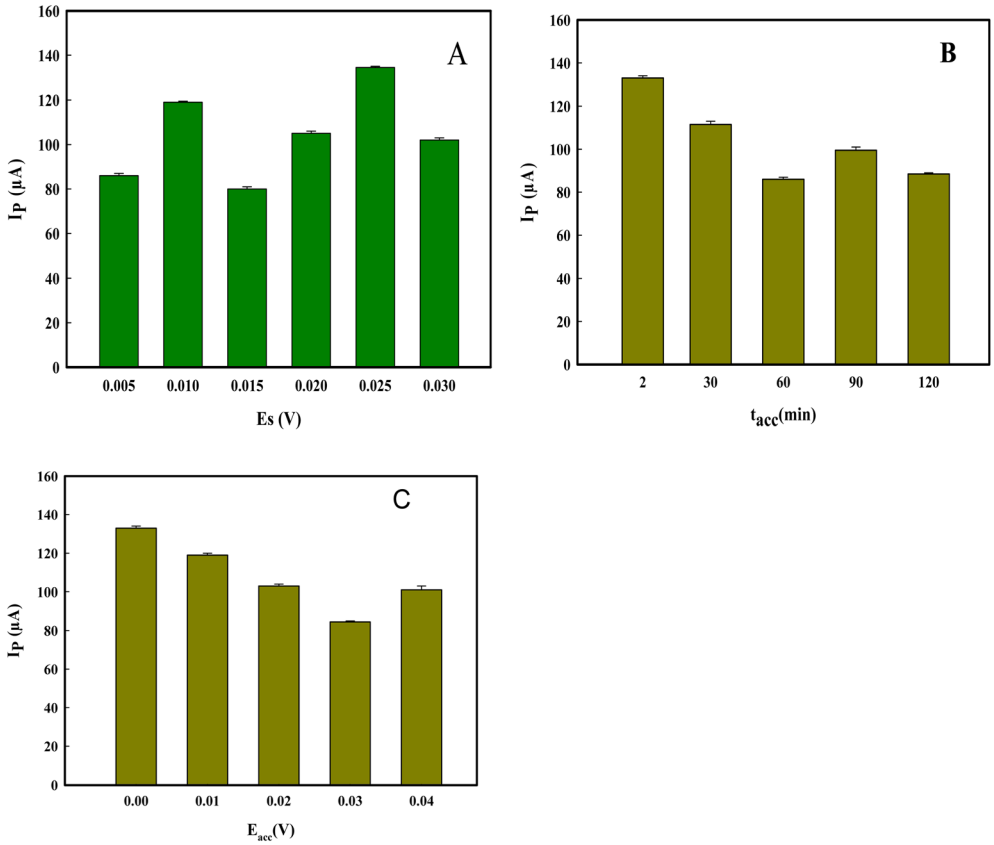

Fig. 3 Effects of (A) potential step, (B) accumulation time, and (C) accumulation potential on the response of the fabricated BGE towards a 10 μM VIN solution prepared in a 0.1 M B–R buffer, pH 6.

After investigation of the modification and operational variables, it can be concluded that the optimal performance of the proposed BGE was attained by a simple two-step modification process, having a sequence of 120 seconds of amperometric deposition of AuNPs followed by eight electropolymerization voltammetric cycles of 2.5 mM DL-met. An t_{acc} of zero s, E_{acc} of zero V, E_s of 0.025 V, pulse amplitude of 0.2 V, pulse duration of 0.02 s, a potential window from 0.4 V to 1.0 V, and a scan rate of 0.05 V s^{-1} were the optimal parameters employed in the DPV detection of VIN in 0.1 M B–R buffer, pH 6.0. All measurements were performed at room temperature.

3.3. Electrochemical characterization of the fabricated sensor

The electroactive surface of the sensor was characterized prior to and at its two modification stages by applying electrochemical impedance spectroscopy (EIS) and cyclic voltammetry (CV) using 5.0 mM $[Fe(CN)_6]^{3-}/[Fe(CN)_6]^{4-}$ (FCN) prepared in 0.1 M KCl as an active redox probe owing to its well-established electrochemical characteristics. EIS measurements were recorded at a constant potential of 0.1 V with an amplitude of 0.01 V and a frequency range of 1.0 Hz–100 KHz, whereas the CV measurements were performed from −0.5 V to 0.8 V, using a potential step of 0.01 V.

EIS is a reliable and powerful approach for examining the interface features of the sensor surface. It was employed for the assessment of the BGE's improved electrochemical conductivity at each modification stage using an FCN probe. The impedance spectra (Nyquist plots), shown in Fig. 4(A), consist of two parts: a semicircle at high frequencies and a linear part at lower frequencies. The diameter of the semicircle portion in the Nyquist plot can be employed to compute the resistance to electron transfer (R_{ct}) at the sensor surface, which regulates the FCN probe's electron transfer kinetics, through its fitting to the Randle circuit, as an equivalent circuit.

It was observed that poly(DL-met)/AuNPs-BGE exhibits the smallest R_{ct} (~154 Ω) compared to other electrodes, while the highest R_{ct} value (~942 Ω) was obtained for the bare electrode, indicating the facilitated charge transfer with poly(met)/AuNP modification. The EIS data obtained serve as a reliable indicator of the relatively high surface conductivity and electroactive sites of the fabricated sensor.

Cyclic voltammograms of the prepared electrodes at 0.1 V s^{-1} scan rate showed two apparent oxidation-reduction peaks that are conformable to FCN reversible electron transfer mechanism. As shown in Fig. 4(B), comparatively shallow cathodic and anodic redox peaks were obtained on the surface of the bare BGE (curve a). The Au-modified sensors showed pronounced electrocatalytic characteristics and quicker electron transfer kinetics at their effective working area, which is evidenced by the clearly visible improvement in the peak intensity upon using the AuNPs-BGE (curve b) compared to the bare BGE. Superior

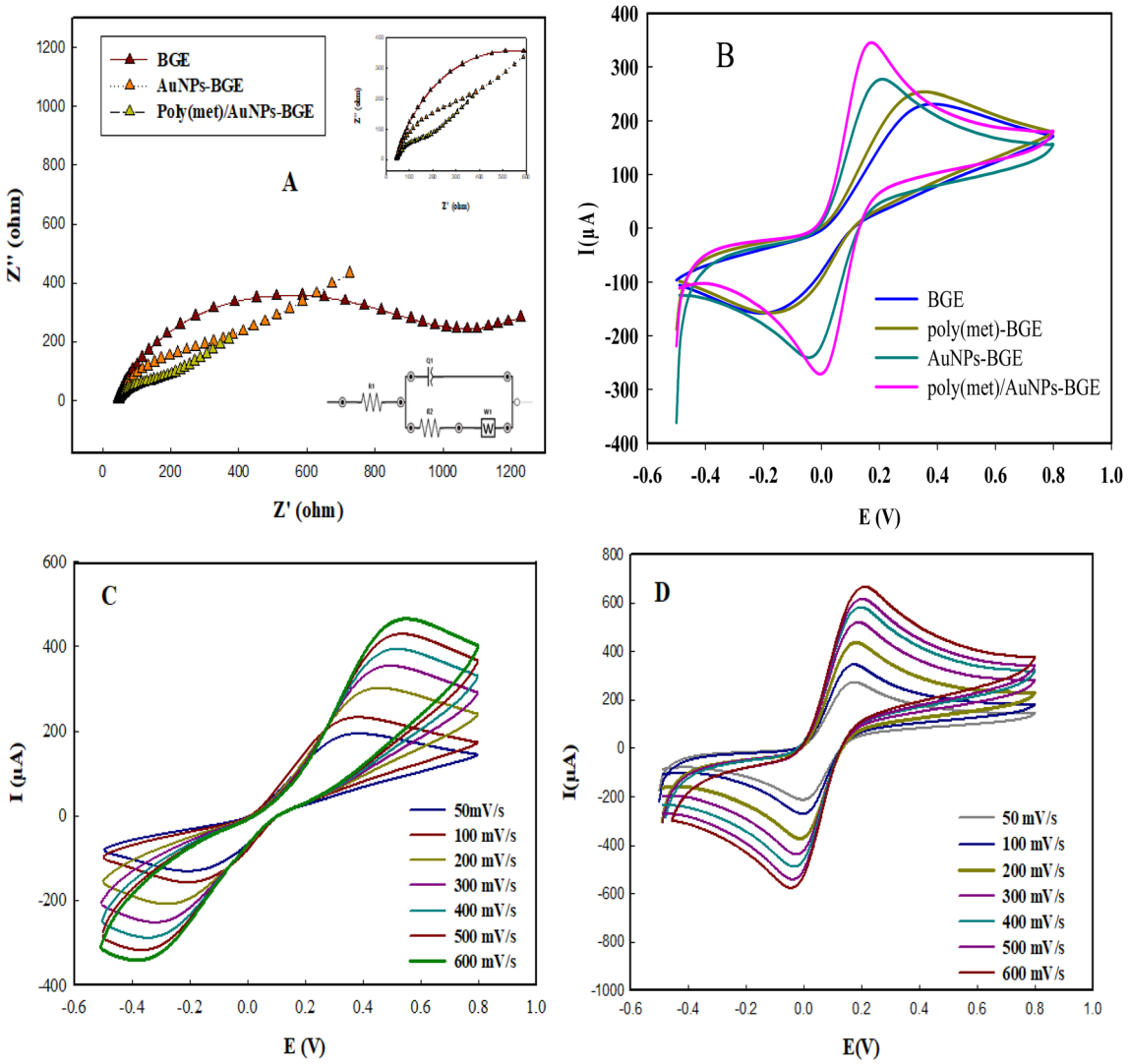

Fig. 4 (A) Nyquist plots of the fabrication steps of the poly(DL-met)/AuNPs-BGE using 5.0 mM FCN at a potential of 0.1 V, a frequency in the range of 1.0 Hz–100 KHz and an amplitude of 0.01 V. (B) CVs of the stepwise fabrication of the presented BGE using 5.0 mM FCN in a 0.1 M KCl solution with a potential window of −0.5 −0.8 V and a potential scan rate of 0.1 V s^{-1} for the (a) bare BGE, (b) AuNPs-BGE, (c) poly (DL-met)/AuNPs-BGE, and (d) poly (DL-met)-BGE. CVs of 5.0 mM FCN in a 0.1 M KCl solution from −0.5 V to 0.8 V at different scan rates from 0.05 V s^{-1} to 0.6 V s^{-1} using the (C) bare BGE, and (D) poly (DL-met)/AuNPs-BGE.

peak characteristics were observed on using poly(DL-met)/AuNPs-BGE (curve c) compared to other electrodes, proving the formation of a conducting polymeric layer with more electroactive sites and thus an increased working area. The CV of poly(DL-met)/BGE (curve d) represents weak redox peaks compared to the Au-modified BGE. This confirms that AuNPs have a potential additive impact on improving the electrocatalytic properties of poly(DL-met) through their effective binding to poly(DL-met) active sites ((–S) and (–NH_2) groups), as reported in the literature.[55]

The bare and poly(DL-met)/AuNPs-BGEs were also characterized for electro-chemically active surface area by tracing their current responses for FCN redox probe applying CV at different potential scan rates ranging from 0.05 to 0.6 V s^{-1}. As indicated in Fig. 4(C), the anodic (I_{pa}) and the cathodic (I_{pc}) peak current responses of bare Fig. 4(C) and poly(DL-met)/AuNPs-BGE, Fig. 4(D) grew continuously and linearly with scan rate. The current recordings (I_p, μA) were plotted against the square roots of the potential scan rate ($\nu^{1/2}$, (mV s^{-1})$^{-1/2}$), yielding straight lines, as represented in Fig. 5(A) for bare BGE and Fig. 5(B) for poly(DL-met)/AuNPs-BGE.[36] The derived regression equations eqn (4) and (5) for poly(DL-met)/AuNPs-BGE are as follows:

$$I_{pa}\ (\mu A) = 21.4294\ \nu^{1/2} + 129.75 \quad R^2 = 0.9983 \tag{4}$$

$$I_{pc}\ (\mu A) = -21.217\ \nu^{1/2} - 111.121 \quad R^2 = 0.9976 \tag{5}$$

Fig. 5(C) also shows a linear relationship between the logarithm of the anodic peak currents (log I_P) and that of the scan rate (log ν) with a linear regression equation (eqn (6)) as follows:

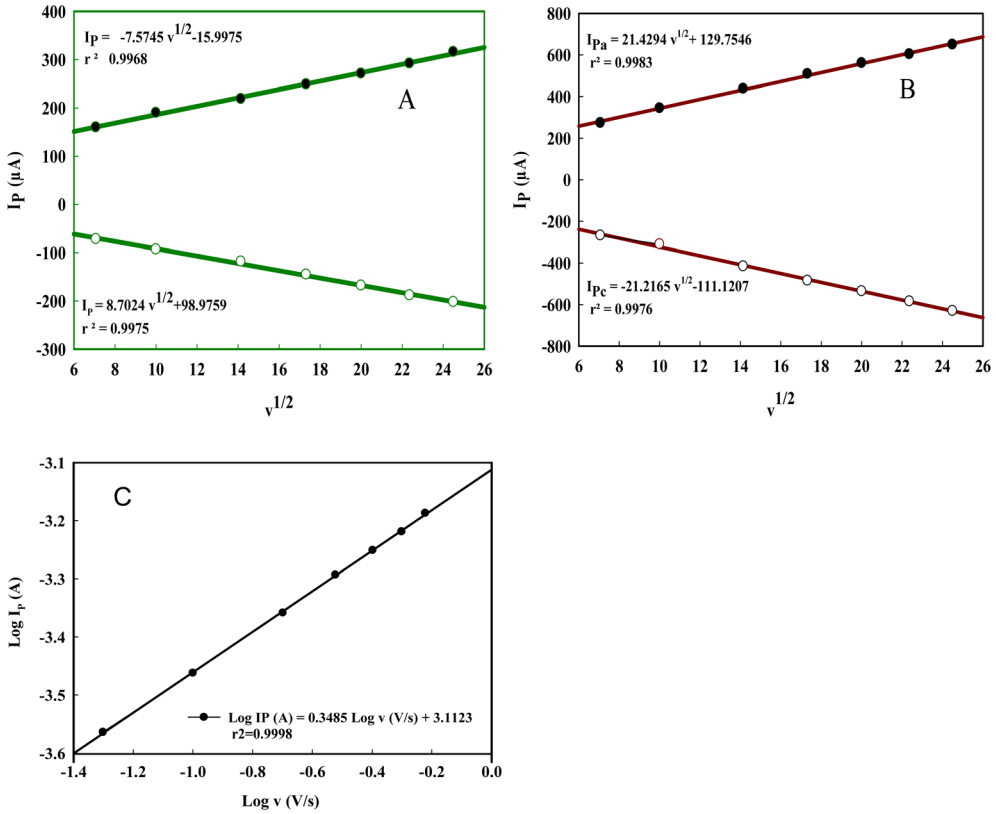

Fig. 5 Anodic and cathodic peak current responses (I_P, μA) of the (A) bare BGE, and (B) poly (DL-met)/AuNPs-BGE towards 5.0 mM FCN in a 0.1 M KCl solution *vs.* square roots of scan rate (mV s^{-1}). (C) Normal logarithm of anodic peak current responses (log I_P, A) of the poly(DL-met)/AuNPs-BGE towards 5.0 mM FCN in a 0.1 M KCl solution *vs.* that of scan rate (log ν, V s^{-1}).

$$(\text{Log } I_{pa}\text{ (A)} = 0.3485 \log \nu\text{ (V s}^{-1}\text{)} + 3.1123) \quad R^2 = 0.9998 \quad (6)$$

The obtained slope, 0.3485 is closely approximate to the claimed value of 0.5 for diffusion-controlled electrochemical reactions.[36,63]

The sensors' functional surface area was estimated from the Randles–Sevcik formula (eqn (7)) for a reversible diffusion controlled process, presented as follows:

$$I_{pa} = (2.69 \times 10^5)\, n^{3/2}\, A\, (D)^{1/2}\, C_o\, \nu^{1/2} \quad (7)$$

where I_{pa} is the maximum oxidation current, n is the number of electrons transferred ($n = 1$), D is the diffusion coefficient (7.6×10^{-6} cm^2 s^{-1}), C_o is the FCN concentration (2.5×10^{-3} M), A is the cited electrode surface area, and $\nu^{1/2}$ is the square root of scan rate.[64] The average electroactive surface area of the bare BGE and poly(DL-met)/AuNPs-BGE were estimated to be 0.081, and 0.189 cm^2, respectively, using the derived slope from the (I_P *vs.* $\nu^{1/2}$) linear relation (eqn (4) and (5)). The manifest increase (~2.5 times) in the working area of the modified sensor compared to the bare one verifies the obvious improvement in the sensor conductivity through providing more active sites for the redox reactions to occur, and greatly accelerating the capacity of electron transport, supporting the EIS findings.

3.4. Morphological characterization studies

The surface morphological characterization of the proposed BGE prior to and after each modification stage was carried out by analyzing the micrographs recorded by AFM and SEM technologies. EDX spectroscopy was also performed for the elemental composition investigation of the sensor after each modification step.

The topographic alteration with the progressive modification steps was investigated, and the associated changes in roughness were calculated using atomic force microscopy (AFM). The corresponding root mean square roughness (R_q) values for BGE, AuNPs-BGE, and poly(DL-met)/AuNPs-BGE were estimated from 0.1 × 0.1 μm (scan area) two-dimensional (2D) and three-dimensional (3D) AFM pictures using the contact mode, as revealed by Fig. 6(Part I). The surface of the bare BGE was relatively smooth, with an R_q value of 2.483 nm (Fig. 6(Part I, A)), while the R_q value of the AuNPs-BGE surface (Fig. 6(Part I, B)) reached 3.821 nm, signifying the more exposed surface area due to AuNPs' deposition as randomly distributed spheres. Furthermore, for the poly(met)/AuNPs-BGE (Fig. 6(Part I, C)), more particles were observed, which might be the outcome of the polymerization of met over the formerly deposited AuNPs with a slightly increased R_q value of 3.929 nm, referring to a pronounced improvement in the electroactive surface area and conductivity owing to the granular polymeric coating

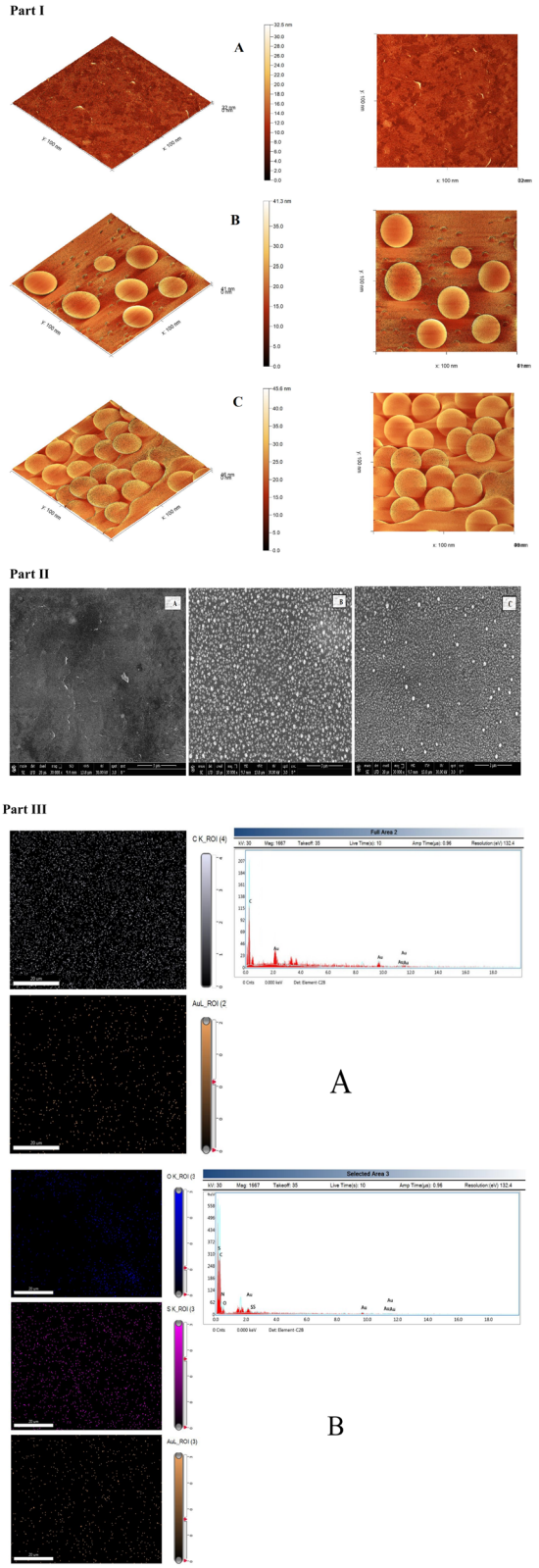

Fig. 6 AFM images (Part I) of the (A) bare BGE, (B) AuNPs-BGE, and (C) poly (DL-met)/AuNPs-BGE. SEM images (Part II) of the (A) bare BGE, (B) AuNPs-BGE, and (C) poly (DL-met)/AuNPs-BGE at a magnification of 30 KX, and EDX mapping (Part III) of the (A) AuNPs-BGE, and (B) poly (DL-met)/AuNPs-BGE.

development of poly(DL-met), which is stabilized by chemical bonding with AuNPs.[65]

For further morphological investigation, Fig. 6(Part II) presents the SEM images of the bare and modified electrodes at specific settings, including a working scale of 3 μm, a stimulation voltage of 30 KV, and a magnification level of 30 KX. Fig. 6(Part II, A) indicates that the surface of the bare BGE is reasonably smooth and clean without any contamination, while Fig. 6(Part II, B) reveals the homogenous dispersion of electro reduced AuNPs as bright tiny amorphous clusters, with an average size of 30 nm. The polymeric coating with poly(DL-met) was displayed as a three-dimensional dense and compact layer with few scattered tiny spots of AuNPs, as shown in Fig. 6(Part II, C), indicating that the electropolymerization of (DL-met) was efficacious.

EDX spectroscopic analysis was performed for the elemental mapping of the sensor surface after each step of modification, as supporting investigational studies. The EDX spectrum for the AuNP-modified sensor has signals corresponding to metallic Au with a percentage of 21.77% (Fig. 6(Part III, A)), confirming the successful deposition of AuNPs on the sensor surface. This illustrates the expanded functional area and the more pronounced conductivity in the analysis that AuNPs provide. While in the spectrum corresponding to poly(met)/Au-NPs BGE, the Au signals were declined, with 1.72%, confirming the uniform coverage of the surface of the Au-NPs/BGE with a uniform layer of poly(DL-met) (Fig. 6(Part III, B)).

3.5. Electrochemical performance and validation of the sensor

The electrochemical response of both the bare and modified BGEs in 0.1 M B–R buffer of pH 6.0 towards 10 μM VIN was investigated after the optimization of all previously mentioned parameters. The impact of modification stages on the electroactivity of the BGE for the determination of VIN was examined employing DPV due to its higher selectivity and sensitivity compared to CV, as reported in the literature.[17,21]

As illustrated in Fig. 7(A), a shallow anodic peak (4 μA) was obtained on the bare BGE (curve a), a slight increase in the oxidation peak current (18 μA) at about 0.76 V was observed for the poly(DL-met)-BGE surface (curve b), while for the Au-modified BGE surface, a well-defined oxidation peak at a much lower potential was observed with a remarkable enhancement of the electrochemical signal of VIN, which demonstrates that the electrodeposition of AuNPs enhances the reaction kinetics owing to their high electrocatalytic activity, and an oxidation peak with a magnitude of 85 μA was developed at 0.69 V on using the AuNPs-BGE (curve c). This agrees with the previously reported results indicating that the deposition of AuNPs on unmodified electrode surfaces supports effective mass transfer, facilitates electron transfer, and increases the electrode's effective area because of the particles' sphere-like shape and high surface-to-volume ratio and, in turn, explains the noticeable improvement in VIN signal.[66,67]

Moreover, the poly(DL-met)/AuNPs-BGE (curve d) showed the highest current intensity (132 μA) compared to the other

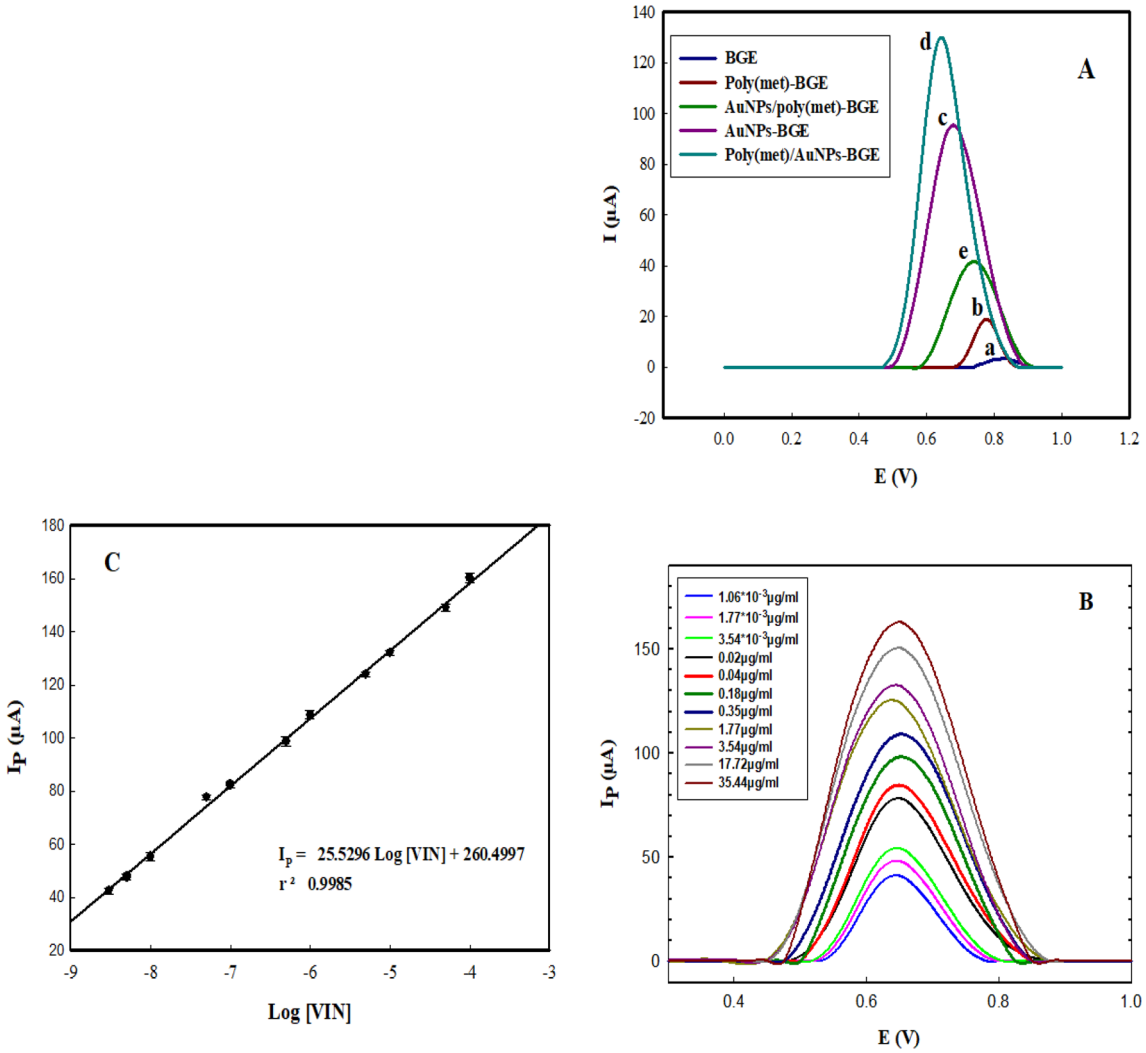

Fig. 7 (A) DPV of 10 μM VIN in B–R buffer at pH 6 on the surface of the bare BGE (a), poly(met)-BGE (b), AuNPs-BGE (c), poly(met)/AuNPs-BGE (d), and AuNPs/poly(met)-BGE (e) from 0.0 to 1.0 V at a scan rate of 0.05 V s^{-1} (B) DP voltammograms for VIN estimation in B–R buffer 0.1 M, pH 6.0 utilizing the proposed poly(met)/AuNPs-BGE, at a scan rate of 0.05 V s^{-1} with working concentrations from 10^{-4} to 3×10^{-9} M (35.44 to 1.06×10^{-3}) μg mL^{-1} of VIN. (C) The corresponding calibration graph for the VIN detection on the fabricated sensor surface.

electrodes. This can be illustrated by the synergistic electrocatalytic influence of poly(DL-met), attached to AuNPs by means of the amide and thioether bonds, enabling the formed polymer to act as a stabilizing agent, as metal nanoparticles solely at the electrode surface may become brittle.[68,69] In addition, AuNPs are able to diffuse throughout the porous polymer matrix, producing more active sites.[70] Consequently, it was suggested that the enhanced electrocatalytic performance of the fabricated sensor results from its improved electron transfer kinetics and increased working surface area, which even serves as an active surface for the analyte's electro-oxidation.

The deposition sequence was also examined, a weak current signal (37 μA) at 0.74 V was observed when VIN was oxidized on the sensor surface with electrodeposited AuNPs over the electropolymerized (DL-met), as shown in curve e; thus, it was not recommended for the surface modification of the presented sensor.

3.6. Calibration graph, detection and quantitation limits

Differential pulse voltammetric measurements of VIN in 0.1 mol L^{-1} B–R buffer of pH 6.0 (Fig. 7(B)) were conducted using the fabricated BGE/AuNPs/poly(DL-met) sensor and the optimized operational conditions. The oxidation peak current responses (I_P, μA) from the baseline for the serially diluted VIN working standards were computed and plotted against the corresponding concentrations (logarithms (log[VIN], M)) to construct a calibration curve for the detection and estimation of trace amounts of VIN in bulk, pharmaceutical formulations and biological samples.

Spanning the wide range from 1.06 ng mL^{-1} to 35.44 μg mL^{-1}, the I_P value showed a linear relationship with log[VIN], as shown in Fig. 7(C), which can be represented by the following regression equation (eqn (8)):

$$I_p\ (\mu A) = 260.53 + 25.53 \log[VIN] \quad (R^2 = 0.9985, n = 3) \quad (8)$$

Table 1 The performance of the suggested sensor in comparison to the previously published techniques

Method	Linear range ($\mu g\ mL^{-1}$)	Detection limit ($\mu g\ mL^{-1}$)	Application	References
HPLC-UV	5.50×10^{-3}–5.00	5.00×10^{-3}	Pharmaceutical manufacturing equipment surface	8
HPLC-UV	1.00×10^{-3}–0.20	3.00×10^{-4}	Human plasma	71
HPLC-UV	2.00–26.00	0.05	Capsule	72
HPLC-UV	2.00–200.00	0.37	Capsule	73
HPLC-MS/MS	1.38×10^{-4}–1.38	9.30×10^{-5}	Plant samples	10
Spectrophotometry	2.00–14.00	0.43	Capsule	73
Spectrofluorimetry	0.05–0.90	1.30×10^{-3}	tablet	11
SW-AdSV (Nujol-based CPE)	3.54×10^{-3}–0.14	1.06×10^{-3}	Capsule and serum	16
DPV (GCE)	0.66–8.36	0.50	Capsule and urine	
SWV (GCE)	1.65–24.75	1.67		
DPV (poly(DL-met)/AuNPs/BGE)	1.10×10^{-3}–35.44	1.61×10^{-4}	Capsule, serum and urine	The present work

The high degree of coefficient of determination ($R^2 = 0.9985$) and low standard deviation values (0.816–1.70) ($n = 3$) confirm the efficiency and accuracy of the suggested technique over the designated concentration range.

The suggested electrochemical method demonstrated a high sensitivity for VIN determination in addition to a short response time and a wide linear range. Based on the signal-to-noise ratio, low values of the limit of quantification (LOQ = 10S/N) and the limit of detection (LOD = 3S/N) were obtained. The signed values of LOD and LOQ were 0.16 ng mL^{-1} and 0.54 ng mL^{-1}, respectively.

The analytical performance characteristics of the proposed technique in terms of sensitivity, linearity, and applicability were compared to those previously reported in the literature.[8,10,11,16,71–73] As illustrated in Table 1, it is obvious that the suggested approach has a much wider linear range and improved sensitivity compared to the reference voltammetric, HPLC-UV, and spectrofluorimetric methods. It also demonstrates a comparable LOD to that of the cited HPLC-MS/MS,[10] which requires trained personnel and sophisticated instrumentation.

The proposed sensor was also found to show superior sensitivity and selectivity for VIN detection over the previously published voltammetric methods, which utilized unmodified carbon paste and glassy carbon electrodes. Moreover, the fabricated BGE has other advantages such as a simpler fabrication procedure than Nujol-based CPE and a lower cost than that of the GCE. This demonstrates the potential efficiency of employing the current sensor for detecting even much lower concentrations of VIN for quality control units and also for the pharmacokinetics evaluation, without requiring the meticulous sampling steps or skilled personnel needed for the costly HPLC technique.

3.7. Repeatability, reproducibility, and stability

The repeatability (intraday precision) and reproducibility (interassay precision) of the proposed sensor have been evaluated as stated by the ICH.[74] The peak current responses for 10 μM VIN using B–R buffer (pH 6.0, 0.1 M), applying DPV under the optimized conditions, were monitored.

The tendency to obtain the same results for a particular analysis method under identical conditions is known as repeatability. Accordingly, the same sensor was utilized five times within the same day to investigate the repeatability (within-day). Reproducibility is related to the potential of obtaining the same estimation outcomes under variable operational conditions for a particular analytical approach. These conditions may include using different instruments, reagents, analysts, or even times and/or locations of the measurement. Thus, the current response was monitored over three successive days, using the same electrode and the optimized experimental variables for testing the reproducibility (between-days). Additionally, the fabrication reproducibility (inter-assay precision) was tested using three different sensors, which were decorated and utilized under the optimal fabrication and operational conditions. The results revealed RSD% values of 1.35, 1.22, and 3.69 for within-day, between-day, and inter-assay precision, respectively, demonstrating satisfactory repeatability and reproducibility of the designed sensor. Over a period of 30 days, the presented sensor was stored at ambient temperature, the sensor's operational shelf stability was monitored at different time intervals, and the differential pulse voltammograms for 10 μM VIN were recorded; consistent and repeatable current responses were observed, with an RSD of 4.34%, confirming the high stability of the fabricated sensor.

3.8. Interference study

The key component of the electrochemical sensor's performance is selectivity. Consequently, a cross-selectivity inspection for a range of moieties that could potentially interfere with VIN measurements, such as piracetam, donepezil, and memantine, as functionally related nootropic agents, vinpocetine, as a structurally related synthetic derivative, and some co-administered drugs, such as pantoprazole and vit B_{12}, was performed.

These constituents' interfering effect was investigated by monitoring the voltammetric response (I_P) of 0.1 μM VIN in a mixture comprising these constituents at different concentration levels (equimolar, 10 folds, and 100 folds that of VIN), using DPV under optimal operational conditions.

Table 2 Effects of the possible interferents on vincamine determination using the proposed BGE. $\%I_p$ change: the relative percent change in current

Interferent	Ratio analyte: interferent	$\%I_p$ change
Piracetam	1 : 1	3.61
	1 : 10	2.41
	1 : 100	4.82
Donepezil	1 : 1	−3.21
	1 : 10	−6.83
	1 : 100	2.01
Memantine	1 : 1	5.62
	1 : 10	3.82
	1 : 100	7.63
Vinpocetine	1 : 1	1.61
	1 : 10	2.81
	1 : 100	6.02
Pantoprazole	1 : 1	−5.22
	1 : 10	−5.82
	1 : 100	−4.82
Vit B_{12}	1 : 1	2.21
	1 : 10	−1.21
	1 : 100	−4.02

The following simple formula (eqn (9)) was utilized to evaluate the outputs:

$$(\%I_p \text{ change} = [(I_{pP} - I_{pM})/I_{pP}] \times 100) \quad (9)$$

where $\%I_p$ change is the relative percent change in current, I_{pP} is the oxidation current of the pure VIN solution, and I_{pM} is the oxidation current of a solution mixture of VIN and interfering species at a specified ratio of analytes to interferents.[17]

The sensor's reactions to the subsequent incorporation of these interferents were essentially insignificant, as shown in Table 2, which revealed that even when the concentration of each interfering species was 100 times higher than that of VIN, the poly(DL-met)/AuNPs-BGE possesses significant tolerance and selective electrocatalytic activity with minimal interference effect on the oxidation of VIN.

3.9. Analytical application of the proposed sensor

Pharmaceutical formulations are usually composed of a variety of excipients; hence, it was crucial to study the reliability and specificity of the proposed approach towards VIN detection in the presence of other encountered additives.

For this purpose, the commercially available Brain-ox® capsules (30 mg VIN per cap) were utilized, and the attained current responses were compared with the previously represented data of pure VIN that the calibration curve showed, utilizing the ultra-sensitive waste battery electrode and the optimal parameters.

The recovery values obtained for all the tested samples fell within the range of 96.39–99.65% with a RSD% range of 0.502–1.29, and a standard error (SE) range of 0.289–0.72, as illustrated by the data listed in Table 3. Based on the satisfactory recovery values, it can be concluded that the suggested BGE/AuNPs/poly(met) sensor can be applied efficiently, yielding a highly accurate and precise assessment of VIN in pharmaceutical samples without interference from any encountered additives or excipients.

For more investigation of the selectivity and applicability of the developed sensor, it was tested in spiked human plasma and urine samples under the optimized experimental settings applying the DPV technique. The recovery ranges of VIN determination in the human plasma and urine samples were 95.78–98.92% and 97.90–101.20%, respectively, with RSD values of 1.62% and 1.78%, respectively.

Table 3 provides an overview of the acquired analytical data, referring to the high degree of specificity of the developed sensor even in the presence of complicated biological matrices. The satisfactory detection outcomes of VIN in human fluids demonstrate that poly(DL-met)/AuNPs-BGE can be applied as an efficient and reliable sensor for detecting the very low concentrations of VIN, even below its physiological C_{max} in plasma and urine, with no need for dealing with matrix challenges or performing intricate sampling procedures. It also indicates the prospective employment of the designed sensor in quality control departments and regulatory organizations with no need for complex setup, skilled analyst or expensive reagents employed by the chromatographic methods that also require complex, laborious sampling procedures.

3.10. Statistical analysis

Student's *t*-test and the *F*-ratio were applied to statistically compare the data obtained for the determination of VIN in the pharmaceutical formulation with that of a previously reported voltammetric method.[16] As illustrated in Table 4, the computed *F* and *t* values were found to be much lower than the theoretical tabulated values; this manifests that the results achieved by the presented sensor do not show any significant differences compared to the reference method's outcomes. This supports the suggested sensor's reliability, accuracy, and precision.

3.11. Sustainability assessment

Using energy-saving devices, promoting the development of solvent-free methods or at least limiting the consumption of harmful chemicals for extraction and sampling processes, and generating the least amount of waste are all encouraged by green analytical chemistry (GAC) as a way to diminish the awful consequences of analytical approaches on the environment and operators.[75] Therefore, it is imperative to develop balanced green strategies with high-quality outcomes to satisfy the trendy GAC requirements.[76] Three indicators, Analytical Greenness Metric (AGREE); the Green Analytical Procedure Index (GAPI) and the Analytical Eco-Scale (AES), were employed in order to assess the ecological friendliness of the suggested approach:

Analytical Greenness Metric (AGREE) is the most prevailing standard for assessing the environmental friendliness of the analytical procedures recently. It is novel, flexible, and easily accessible free software designed by Pena-Pereira and his co-workers in 2020.[77] It covers all the twelve principles of GAC providing a colourful pictogram (graph resembling a clock), comprising subsections with colours progressing from intense

Table 3 Analytical application of the proposed sensor for the determination of VIN in pharmaceutical formulations, spiked human plasma and urine samples[a]

Sample	Claimed (ng mL^{-1})	Found (ng mL^{-1})	Recovery%	RSD%
BRAIN-OX® 30 mg per cap	35.40	35.20	99.29	0.95
	17.76	17.30	97.42	0.51
	3.54	3.42	96.39	1.29
	1.78	1.77	99.65	0.50
Human plasma	17.76	17.57	98.92	1.72
	3.54	3.40	95.78	0.98
	1.78	1.73	97.20	1.28
Human urine	17.76	17.50	98.49	1.91
	3.54	3.59	101.20	2.13
	1.78	1.74	97.90	1.62

[a] RSD: relative standard deviation ($n = 3$).

Table 4 Statistical comparison of the outcomes of the developed DPV and the reported SW-AdS voltammetric method for the assessment of VIN in BRAIN-OX® capsules[a]

Parameter	Proposed DPV method	Reference SWV method[16]
Mean (%R)	98.19	99.61
Variance	2.40	1.01
n	4	3
Student's t-test		1.31
F-ratio		0.33

[a] The theoretical t and F values at 95% confidence limit, $P = 0.05$, are (2.57) and (9.55), respectively.

green to deep red, the degree of the colour rises as the impact of the evaluated item increases, and a numerical score shown in the centre as a fractional value ranging from zero to one (ideal score) representing the final result. The presented protocol achieved a score of 0.81 with a pictogram having no red segments, as represented in Fig. 8(A), demonstrating an excellent green approach.

The Green Analytical Procedure Index (GAPI) is a comprehensive and reliable tool providing both fundamental qualitative information and precise semi-quantitative information regarding the ecological impact of the entire analytical process.[78] The GAPI pictogram is represented as five main segments (pentagrams), comprising fifteen unique attributes. Each was depicted using a three-tier colour gradient (green, yellow, or red), that spans from significant (red) to minimal environmental impacts (green). The proposed approach exhibited an organic solvent free methodology with a quick analysis time, low power use, minimal waste generation, straightforward processes without tedious preparatory procedures or specific storage conditions for samples, and a portable device. The environmental sustainability of the suggested approach was verified by the GAPI pictogram displayed in Fig. 8(B).

The Analytical Eco-Scale (AES) is an earlier semi quantitative assessment technique that determines the greenness of an operation in terms of energy consumed, waste produced, and reagents employed, taking into account their signal word and number of pictograms specified in "The Globally Harmonized System of Classification and Labelling of Chemicals" (GHS), as well as the labelled safety data sheet for each chemical utilized by the investigated approach.[79] The eco-scale score was calculated by deducting penalty point scores from 100 (ideal value). Green approaches that were deemed good are scored 50 or higher, while those that acquired a score of 75 or higher are considered excellent. The proposed strategy was deemed an excellent green approach, achieving a high score of 85, as shown in Table S1.

Metrics like AGREE, GAPI, and AES concentrate on evaluating the ecological sustainability and greenness, while the blue applicability grade index (BAGI) strikes a compromise between the effectiveness and functionality of analytical practices.[80] A newly developed, simple, and quick tool called BAGI offers an inclusive quantitative mechanism for assessing the applicability "blueness" of analytical techniques. The term "blueness" describes how beneficial and appropriate an analytical technique is for its intended purpose based on important practical aspects.

The BAGI tool considers ten essential practical attributes to enable a thorough evaluation of the practicality, accessibility, and economic benefits of an analytical method. These parameters include the analysis type, the number of chemical moieties to be analysed, the accessibility of equipment used, sample throughput, sampling needs, the analysis speed, the availability of reagents utilized, the degree of automation, and the required sample volume. A scale ranging from 1 (inappropriate) to 10 (optimal) is utilized to evaluate each of these ten qualities. The approximate mean of the ten distinct aspect ratings is calculated to derive the overall BAGI score. Each attribute is visually represented as a part of an asteroid pictogram with a colour ranging from white (worst) to intense blue (best) depending on the gained score.

With a high BAGI score of 77.5, the suggested approach revealed a remarkable blueness with only one white attribute corresponding to single element analysis, as illustrated in Fig. 8(C). The BAGI evaluation shows that our approach holds

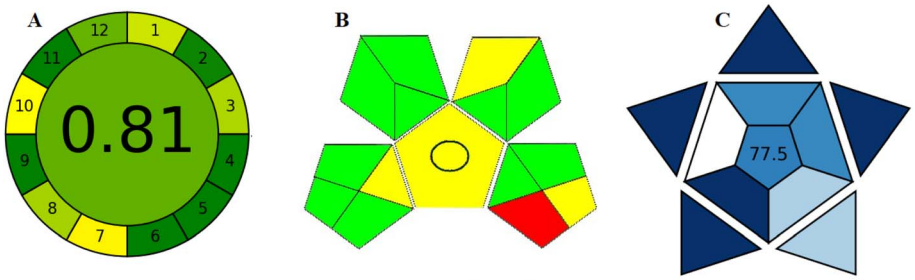

Fig. 8 Greenness evaluation pictograms by: (A) AGREE and (B) GAPI assessment metrics, and (C) practicality evaluation pictogram by the BAGI assessment metric.

significant benefits in terms of practicality, applicability, hazard elimination, and time and cost savings.

4. Conclusion

Electrochemical sensors are rapid, portable, cost-effective, eco-friendly, and highly sensitive devices designed to detect and measure various analytes in samples from environmental, food, pharmaceutical, and other domains. A highly sensitive, sustainable, simple and selective electrochemical sensor, based on the disposable graphite rods from spent batteries modified with poly(met)/AuNPs, is presented and employed for differential pulse voltammetric determination of VIN in bulk, pharmaceutical dosage form, spiked human serum and urine samples. The electrochemical performance outcomes showed that the modified surface's working area was 2.5 times higher than that of bare BGE confirming accelerated charge transfer and significant electrocatalytic effect. The wide working range of linearity from 3.0×10^{-9} to 1.0×10^{-4} M with a high correlation coefficient of 0.9985 and low detection limit of 4.55×10^{-10} M of such green, and cheap sensor bringing it into compliance with the pharmacokinetic evaluation and quality control studies for VIN in a very straightforward manner with no need for dealing with matrix challenges or performing intricate sampling procedures or requiring a complex setup. The suggested organic solvent-free approach demonstrated considerable environmental friendliness, efficiency, and practicality as demonstrated by all applied greenness and blueness assessment tools.

Ethics statement

The authors declare that no *in vivo* experiments were conducted directly on humans and that all the used biological samples used were provided by professionally certified technicians at the El Hayah Private Clinical Laboratory, Giza, from anonymous volunteers, and were handled and discarded according to the ethical regulations of the Faculty of Science, Cairo University.

Conflicts of interest

The authors declare that they have no known competing financial interests or personal relationships that could have appeared to influence the work reported in this paper.

Data availability

The data will be made available from the corresponding author upon request.

Supplementary information: Table 1: the analytical eco scale evaluation of the proposed method. See DOI: https://doi.org/10.1039/d5ra07233f.

References

1 J. C. Depresseux, *Eur. Neurol.*, 2008, **17**, 100–107.
2 P. Wang, C. Chen and M. Shan, *J. Biochem. Mol. Toxicol.*, 2024, **38**, e23714.
3 R. Alaaeldin, Y. A. Eisa, M. A. El-Rehany and M. Fathy, *Naunyn-Schmiedeberg's Arch. Pharmacol.*, 2024, **397**, 7981–7994.
4 H. S. Nandini and P. R. Naik, *Eur. J. Pharmacol.*, 2019, **843**, 233–239.
5 Y. Ren, K. DeRose, L. Li, J. C. Gallucci, J. Yu and A. Douglas Kinghorn, *Bioorg. Med. Chem.*, 2023, **92**, 117439.
6 P. Puech and P. Gallay, *Therapeutics in Cardiology*, 2012, vol. 81, p. 46.
7 Y. A. Sharaf, N. M. Refay, H. E. Abdellatef and N. A. S. Kabil, *Sustainable Chem. Pharm.*, 2024, **42**, 101803.
8 I. Rubashvili, N. Kharukhnishvili and K. Makharadze, *Rev. Roum. Chim.*, 2018, **63**, 205–215.
9 S. S. Mourad, M. A. Barary and A. F. El-Yazbi, *BMC Chem.*, 2024, **18**, 197.
10 J. Liu, Y. Liu, Y.-j. Pan, Y.-G. Zu and Z.-H. Tang, *Anal. Lett.*, 2016, **49**, 1143–1153.
11 F. A. Ibrahim, A. M. Elbrashy, J. J. M. Nasr and M. M. Badr El-Dien, *J. Lumin.*, 2017, **32**, 555–563.
12 N. Mansour, D. El-Sherbiny, F. Ibrahim and H. El-Subbagh, *Ann. Pharm. Fr.*, 2022, **80**, 885–896.
13 S.-M. Sehner and M. Melzig, *Int. J. Pharm. Sci.*, 2022, **77**, 2–5.
14 S. S. Mourad, M. A. Barary and A. F. El-Yazbi, *BMC Chem.*, 2024, **18**, 197.
15 S. R. Al-Mhyawi, M. Abdel-Hamied Abdel-Tawab and R. M. El Nashar, *Food Chem.*, 2023, **411**, 135506.
16 A. M. Beltagi, *Chem. Pharm. Bull.*, 2008, **56**, 1651–1657.
17 K. Vural, S. Karakaya, D. G. Dilgin, H. İ. Gökçel and Y. Dilgin, *Microchem. J.*, 2023, **184**, 108195.

18 P.-A. Le, N. T. Nguyen, P. L. Nguyen and T. V. B. Phung, *Energy Fuels*, 2023, **37**, 7062–7070.
19 T. T. T. Vuong, P. L. Nguyen, N. T. Nguyen, T. V. B. Phung and P.-A. Le, *ACS Omega*, 2024, **9**, 22543–22556.
20 K. k. Chinnakutti, H. Yun, S. Kheawhom, H. Gao, N. Tapia-Ruiz, P. Kidkhunthod, S. Nijpanich, Y. Sawada, N. Saito and J. Kasemchainan, *J. Energy Storage*, 2025, **134**, 118244.
21 H. S. Tawfik, R. A. Ahmed, N. Abdel Ghani and R. M. El Nashar, *J. Electrochem. Soc.*, 2024, **171**, 117503.
22 K. P. Moulya, J. G. Manjunatha, S. A. Aldossari, S. Mohammad and N. Ataollahi, *Top. Catal.*, 2026, **69**, 259–271.
23 M. H. Kabir, M. Y. Pabel, N. T. Bristy, M. A. Salam, M. S. Bashar and S. Yasmin, *RSC Adv.*, 2024, **14**, 36073–36083.
24 S. T. Palisoc, E. J. F. Cansino, I. M. O. Dy, C. F. A. Razal, K. C. N. Reyes, L. R. Racines and M. T. Natividad, *Sens. Biosens. Res.*, 2020, **28**, 100326.
25 V. Selvamani, W. Tejangkura and M. Sawangphruk, *ACS Omega*, 2020, **5**, 15240–15246.
26 K. Moulya, J. Manjunatha, S. A. Aldossari, S. Mohammad and N. Ataollahi, *Top. Catal.*, 2025, 1–13.
27 R. M. Silva, G. H. Sperandio, A. D. da Silva, L. L. Okumura, R. C. da Silva, R. P. L. Moreira and T. A. Silva, *Microchim. Acta*, 2023, **190**, 273.
28 Ž. Z. Tasić, M. B. P. Mihajlović, M. B. Radovanović, A. T. Simonović, D. V. Medić and M. M. Antonijević, *Sci. Rep.*, 2022, **12**, 5469.
29 M. B. Radovanović, A. T. Simonović, M. B. Petrović Mihajlović, Ž. Z. Tasić and M. M. Antonijević, *Chemosensors*, 2025, **13**, 282.
30 S. Alva, P. Septyanda, A. Burhanudin, D. S. Khaerudini, S. N. A. Jenie, R. Sundari and K. Suhud, *ECS J. Solid State Sci. Technol.*, 2023, **12**, 057010.
31 W. Bouali, N. Erk, G. Kholafazadehastamal, M. Naser and G. Tiris, *Diamond Relat. Mater.*, 2023, **131**, 109609.
32 M. Shah, P. Kolhe and S. Gandhi, *Chemosphere*, 2023, **321**, 138148.
33 K. M. Abd-Elsabur, M. Abd-Elsabour, F. H. Assaf and I. M. Hasan, *Electrocatalysis*, 2023, **14**, 875–890.
34 D. Ilager, B. Kurangi, S. S. Jalalpure, S. Pandiaraj, A. N. Alodhayb, K. Mondal, M. A. Alshehri and N. P. Shetti, *J. Mol. Struct.*, 2025, **1335**, 141967.
35 R. S. S. Sahayaraj, R. Sundaresan, S.-M. Chen, B. Ramachandran and N. Chandrasekar, *Chemistry of Inorganic Materials*, 2023, **1**, 100006.
36 M. R. El Naggar, H. M. Fahmy and R. M. El Nashar, *Microchem. J.*, 2024, **206**, 111519.
37 H. R. A. Hasanjani and K. Zarei, *J. Iran. Chem. Soc.*, 2021, **18**, 1613–1623.
38 M. I. Anik, N. Mahmud, A. Al Masud and M. Hasan, *Nano Sel.*, 2022, **3**, 792–828.
39 Z. Hua, T. Yu, D. Liu and Y. Xianyu, *Biosens. Bioelectron.*, 2021, **179**, 113076.
40 S. Ponnada, M. S. Kiai, S. Yadav, A. Palariya, C. S. R. Vusa, R. S. C. Bose, A. Nehra, S. Datta, R. Pawar and G. S. Martynkova, *Appl. Mater. Today*, 2024, **39**, 102310.
41 C. Weber, N. Strom and O. Simoska, *Nanoscale*, 2024, **16**, 16204–16217.
42 S. Mahalakshmi and V. Sridevi, *Electrocatalysis*, 2021, **12**, 415–435.
43 S. Ramanavicius and A. Ramanavicius, *Polymers*, 2020, **13**, 49.
44 A. V. Maksimkin, T. Dayyoub, D. V. Telyshev and A. Y. Gerasimenko, *Nanomaterials*, 2022, **12**, 2272.
45 P. Naskar, A. Maiti, P. Chakraborty, D. Kundu, B. Biswas and A. Banerjee, *J. Mater. Chem. A*, 2021, **9**, 1970–2017.
46 B. Rivkin, C. Becker, F. Akbar, R. Ravishankar, D. D. Karnaushenko, R. Naumann, A. Mirhajivarzaneh, M. Medina-Sánchez, D. Karnaushenko and O. G. Schmidt, *Adv. Intell. Syst.*, 2021, **3**, 2000238.
47 Z. Song, Y. Ma, A. Morrin, C. Ding and X. Luo, *TrAC, Trends Anal. Chem.*, 2021, **135**, 116155.
48 S. Bonyadi and K. Ghanbari, *Mater. Chem. Phys.*, 2021, **267**, 124683.
49 M. El Rhazi, S. Majid, M. Elbasri, F. E. Salih, L. Oularbi and K. Lafdi, *Int. Nano Lett.*, 2018, **8**, 79–99.
50 H. K. Kordasht, M. Hasanzadeh, F. Seidi and P. M. Alizadeh, *TrAC, Trends Anal. Chem.*, 2021, **140**, 116279.
51 A. Raza, S. Javed, M. Z. Qureshi, M. U. Khan and M. S. Khan, *Appl. Nanosci.*, 2017, **7**, 429–437.
52 H. Chen, C. Zhao, Y. Li, J. Li, W. Cai, Y. Kong and Z.-Z. Yin, *J. Electroanal. Chem.*, 2023, **942**, 117562.
53 K. L. Ng, S. M. Lee, S. M. Khor and G. H. Tan, *Anal. Sci.*, 2015, **31**, 1075–1081.
54 S. T. Palisoc, E. J. F. Cansino, I. M. O. Dy, C. F. A. Razal, K. C. N. Reyes, L. R. Racines and M. T. Natividad, *Sens. Bio-Sens. Res.*, 2020, **28**, 100326.
55 D. E. Bayraktepe, E. K. İnal and Z. Yazan, *Microchem. J.*, 2021, **171**, 106812.
56 Y.-P. Juan and T.-H. Tsai, *J. Chromatogr. A*, 2005, **1088**, 146–151.
57 M. Shamsipur, R. Saber and M. Emami, *Anal. Methods*, 2014, **6**, 7038–7045.
58 M. F. Ali and F. A. Abdel-Aal, *RSC Adv.*, 2019, **9**, 4325–4335.
59 A. B. Ahmed, M. M. Abdelrahman, N. S. Abdelwahab and F. M. Salama, *J. AOAC Int.*, 2019, **99**, 1490–1498.
60 P. H. Rieger, in *Electrochemistry*, ed. P. H. Rieger, Springer Netherlands, Dordrecht, 1994, pp. 1–58, DOI: 10.1007/978-94-011-0691-7_1.
61 M. G. Metwally, O. R. Shehab, H. Ibrahim and R. M. El Nashar, *J. Environ. Chem. Eng.*, 2022, **10**, 107699.
62 A. Adenier, M. M. Chehimi, I. Gallardo, J. Pinson and N. Vila, *Langmuir*, 2004, **20**, 8243–8253.
63 M. A. A. Fatah, M. G. Abd El-Moghny, M. S. El-Deab and R. M. El Nashar, *Food Chem.*, 2023, **404**, 134708.
64 A. S. Abo Elalaa, M. Abdel-Hamied Abdel-Tawab, N. T. Abdel Ghani and R. M. El Nashar, *Electroanalysis*, 2022, **34**, 1802–1820.
65 R. Ojani, J.-B. Raoof, A. A. Maleki and S. Safshekan, *Chin. J. Catal.*, 2014, **35**, 423–429.
66 S. Aralekallu and L. K. Sannegowda, in *Handbook of Nanomaterials for Sensing Applications*, ed. C. M. Hussain

and S. K. Kailasa, Elsevier, 2021, pp. 589–629, DOI: 10.1016/B978-0-12-820783-3.00001-4.
67 M. Zamani, N. Tavakkoli and N. Soltani, *Diamond Relat. Mater.*, 2023, **136**, 109954.
68 H. R. A. Hasanjani and K. Zarei, *Biosens. Bioelectron.*, 2019, **128**, 1–8.
69 S. R. Al-Mhyawi, R. K. Ahmed and R. M. El Nashar, *Polymers*, 2021, **13**, 3981.
70 A. Aijaz and Q. Xu, *J. Phys. Chem. Lett.*, 2014, **5**, 1400–1411.
71 L. Dal Bo, G. Ceriani and G. Broccali, *J. Chromatogr. B:Biomed. Sci. Appl.*, 1992, **573**, 158–162.
72 O. M. El-Houssini and M. A. Mohammad, *J. AOAC Int.*, 2022, **105**, 957–963.
73 Y. S. I. El-Saharty, *J. AOAC Int.*, 2019, **91**, 311–321.
74 ICH, *International Conference on Harmonisation*, Geneva, 2005, https://www.ich.org.
75 Y. A. Sharaf, N. Mousad, H. E. Abdellatef and N. A.-S. Kabil, *Anal. Methods*, 2025, **17**, 1252–1264.
76 P. Anastas and N. Eghbali, *Chem. Soc. Rev.*, 2010, **39**, 301–312.
77 F. Pena-Pereira, W. Wojnowski and M. Tobiszewski, *Anal. Chem.*, 2020, **92**, 10076–10082.
78 J. Płotka-Wasylka, *Talanta*, 2018, **181**, 204–209.
79 A. Gałuszka, Z. M. Migaszewski, P. Konieczka and J. Namieśnik, *TrAC, Trends Anal. Chem.*, 2012, **37**, 61–72.
80 N. Manousi, W. Wojnowski, J. Płotka-Wasylka and V. Samanidou, *Green Chem.*, 2023, **25**, 7598–7604.